Wave-Maintained Annular Modes of Climate Variability*

VARAVUT LIMPASUVAN AND DENNIS L. HARTMANN

Department of Atmospheric Sciences, University of Washington, Seattle, Washington

(Manuscript received 15 July 1999, in final form 19 January 2000)

ABSTRACT

The leading modes of month-to-month variability in the Northern and Southern Hemispheres are examined by comparing a 100-yr run of the Geophysical Fluid Dynamics Laboratory GCM with the NCEP–NCAR reanalyses of observations. The model simulation is a control experiment in which the SSTs are fixed to the climatological annual cycle without any interannual variability. The leading modes contain a strong zonally symmetric or annular component that describes an expansion and contraction of the polar vortex as the midlatitude jet shifts equatorward and poleward. This fluctuation is strongest during the winter months. The structure and amplitude of the simulated modes are very similar to those derived from observations, indicating that these modes arise from the internal dynamics of the atmosphere.

Dynamical diagnosis of both observations and model simulation indicates that variations in the zonally symmetric flow associated with the annular modes are forced by eddy fluxes in the free troposphere, while the Coriolis acceleration associated with the mean meridional circulation maintains the surface wind anomalies against friction. High-frequency transients contribute most to the total eddy forcing in the Southern Hemisphere. In the Northern Hemisphere, stationary waves provide most of the eddy momentum fluxes, although high-frequency transients also make an important contribution. The behavior of the stationary waves can be partly explained with index of refraction arguments. When the tropospheric westerlies are displaced poleward, Rossby waves are refracted equatorward, inducing poleward momentum fluxes and reinforcing the high-latitude westerlies. Planetary Rossby wave refraction can also explain why the stratospheric polar vortex is stronger when the tropospheric westerlies are displaced poleward. When planetary wave activity is refracted equatorward, it is less likely to propagate into the stratosphere and disturb the polar vortex.

1. Introduction

Recent observations demonstrate that month-to-month tropospheric variation in the Northern Hemisphere is dominated by a mode that has a strong zonally symmetric or *annular* component (Baldwin and Dunkerton 1999; Thompson and Wallace 1998, 2000, hereafter TW). The zonal mean part of the Northern Hemisphere variability is remarkably similar to that of the annular atmospheric variability in the Southern Hemisphere (e.g., Trenberth 1984; Yoden et al. 1987; Kidson 1988; Shiotani 1990; Nigam 1990; Karoly 1990; Hartmann and Lo 1998). In particular, despite contrasting land–sea distribution, the zonally symmetric component of the Northern and Southern Hemisphere annular modes (hereafter NAM and SAM, respectively) describes a north–south movement of the midlatitude zonal jet in which the anomalous structure exhibits a dipole pattern in westerly winds with centers at high (50°–60°) and low (30°–40°) latitudes. By convention, the index (i.e., time series) of the annular mode is positive (''high'' phase) when the zonal jet is displaced poleward from its climatological position. During the low phase, the jet shifts equatorward. The polar vortex expands and contracts in relation to the varying jet position.

In the Southern Hemisphere (SH), the annular mode of variability is associated with the low-frequency zonal mean zonal wind ($\overline{u}$) vacillation between 40° and 60°S. This fluctuation is relatively easy to simulate in atmospheric models and has been shown to result from the interaction between transient eddies and zonal mean flow (e.g., Robinson 1991; Yu and Hartmann 1993). Since stationary wave features are weak in the SH, the eddy interaction with the zonal flow is contributed almost entirely by transient waves resulting from the instability of the zonal mean flow. Hartmann (1995) and Hartmann and Lo (1998) observe that synoptic wave structures vary with the zonal mean flow, and the eddy momentum fluxes associated with these changed structures tend to reinforce the zonal wind variations.

In the Northern Hemisphere (NH), the variable be-

* Joint Institute for the Study of the Atmosphere and Ocean Contribution Number 703.

Corresponding author address: Varavut Limpasuvan, Department of Chemistry and Physics, Coastal Carolina University, P.O. Box 261954, Conway, SC 29528.
E-mail: var@coastal.edu

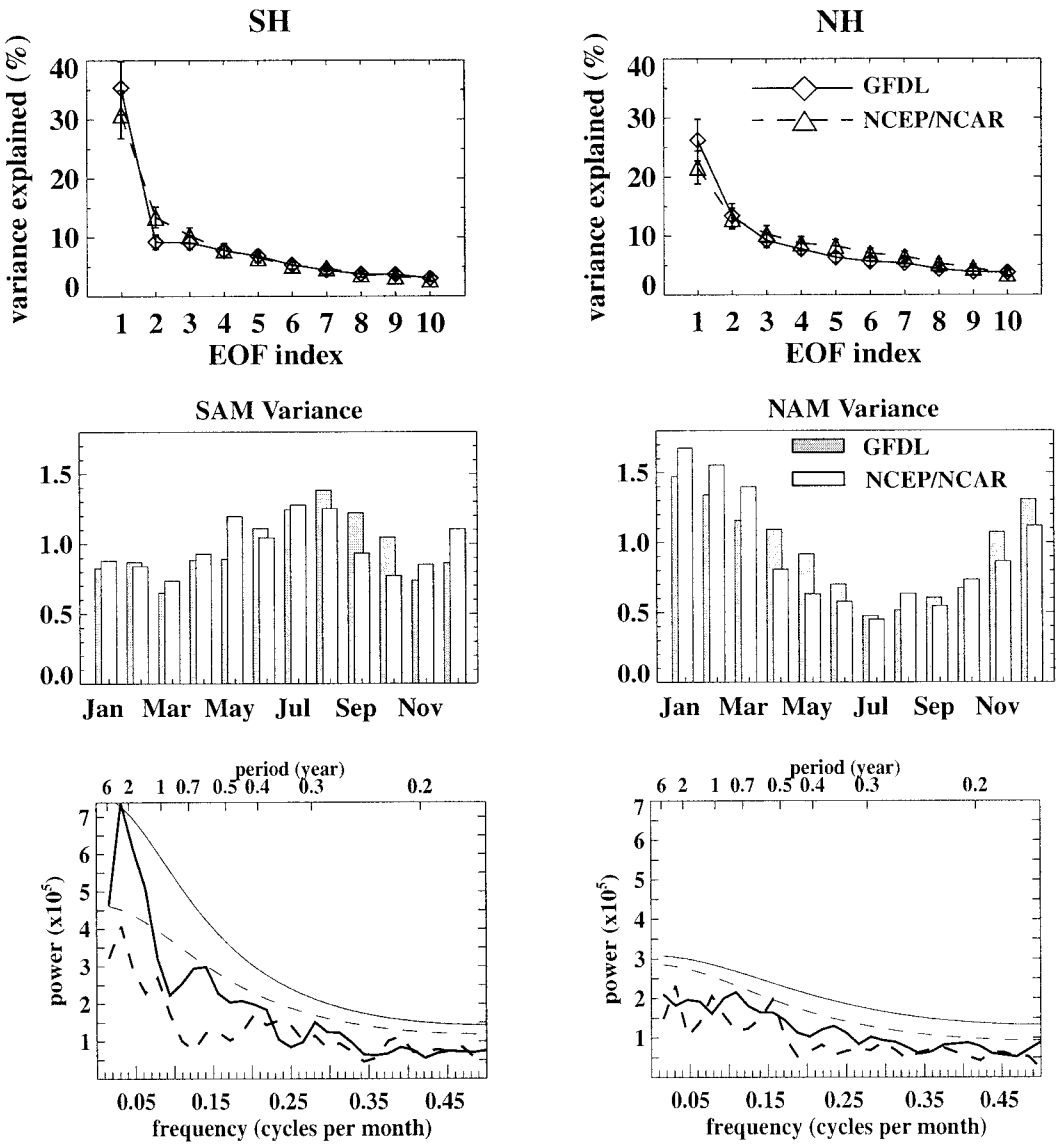

FIG. 1. (top) Fraction of the total variance explained by the first 10 EOFs of the 1000-hPa geopotential height monthly mean anomalies in the (left) Southern and (right) Northern Hemispheres. The normalized PC of the leading EOF serves as the index of the annular modes (SAM and NAM). Dashed (solid) line represents the NCEP–NCAR reanalyses (GFDL model) result. (middle) The annual cycle of the annular mode index variance. Unfilled (filled) bar represents the NCEP–NCAR reanalyses (GFDL model) result. At each month, the bars are slightly displaced to facilitate comparison. (bottom) Power spectra ($\times 10^5$) of the annular mode index for the GFDL output (thick solid line) and the NCEP–NCAR reanalyses (thick dashed line). The thin solid (dashed) line represents the 95% confidence level for the model (reanalyses) spectra. The bandwidth for both is about 0.016 month^{-1}.

havior of the vortex as characterized by NAM [also referred to as the ''Arctic oscillation'' (AO)] has been related to the extratropical winter climate variability expressed by changes in the stationary wave structure (e.g., Wallace and Hsu 1985; Ting et al. 1996). Recent works of Hoerling et al. (1995), Ting et al. (1996), and DeWeaver and Nigam (2000b) suggest that low-frequency fluctuations in the climatological $\overline{u}$ between roughly 35° and 55°N can account for much of the wintertime stationary wave variability at several geographical regions. The underlying reason is that anomalous $\overline{u}$ can induce a large anomalous stationary wave response through linear zonal–eddy interactions. The induced changes in stationary waves are largely independent from the effects of El Niño–Southern Oscillation.

Based on the sea level pressure (SLP) meridional difference across the North Atlantic (e.g., between observational stations at Lisbon, Portugal, and Stykkisholmur, Iceland), the traditional North Atlantic oscillation (NAO) index has also been used to characterize much of the winter-to-winter variability in the Northern Hemi-

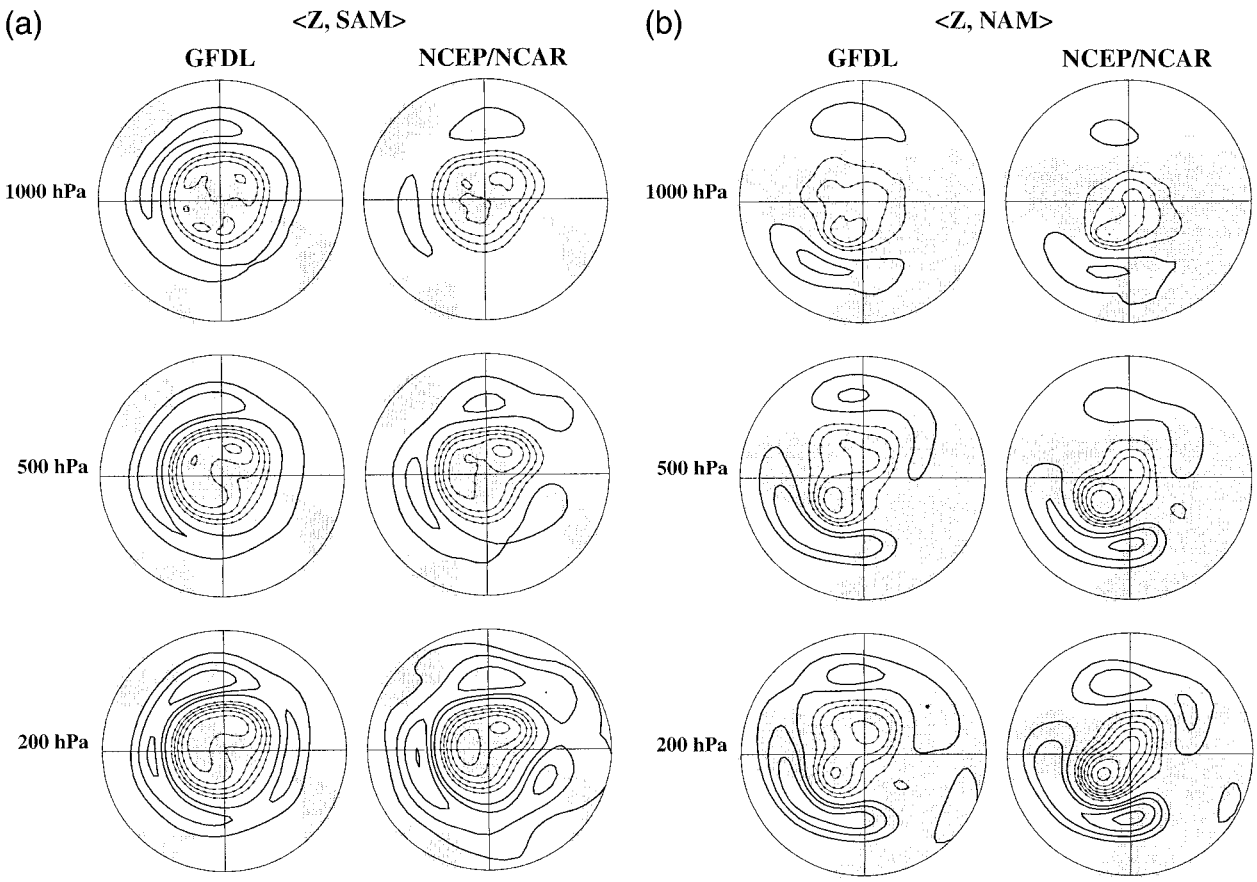

FIG. 2. (a) Geopotential height anomalies associated with the Southern Hemisphere annular mode (SAM) at three levels for the (left) GFDL model and (right) NCEP–NCAR reanalyses results. These patterns are shown as regression maps of the monthly geopotential height anomalies (Z) onto the annular mode index. Negative (positive) anomalies are given by connected dashed (solid) contours. The zero contour is omitted. The contour interval is 10 m per standard deviation of the index. (b) Same as Fig. 2a except for the Northern Hemisphere annual mode (NAM).

sphere (e.g., Rodgers 1984). Hurrell (1995) noted that a bias toward the high NAO phase since the late 1960s may be implicated in the climatic trend over the North Atlantic and Eurasia. Recently, Thompson et al. (2000) demonstrated however that this climatic trend can be better resolved with the NAM index, which also shows preference toward its high state during the past 30 yr. As discussed by Wallace (2000), the spatial signatures of the NAM and the NAO are virtually indistinguishable. And while the correlation between the historical, station-based NAO index and the NAM index can be low, the correspondence between the NAM index and the ''optimized'' NAO index (derived by projecting the NAO spatial pattern onto the SLP field) is nearly perfect. In this study, we consider the NAO, the AO, and the NAM to be the same phenomenon.

The annular modes appear to be natural or internal modes of the atmosphere. In other words, the associated vortex fluctuation occurs as a result of internal atmospheric dynamical processes. Analyses of the NH variability by Limpasuvan and Hartmann (1999; hereafter LH) and DeWeaver and Nigam (2000a; hereafter DN), as well as previously cited studies of the SH flow vacillation, suggest that external forcing is not required to sustain the annular modes of variability in either hemisphere. However, these modes may be sensitive to external forces due, for example, to ozone depletion and/or global warming (Hartmann et al. 2000; and references therein).

In this paper, we extend the work of LH in documenting the structure and dynamical maintenance of annular modes. We also confirm that these annular modes are indeed internal by demonstrating similarities in their structures when derived using observations and output from a realistic general circulation model (GCM) that excludes external forcing. Overall, the analyzed results show that momentum forcing by eddy fluxes sustains the annular wind, temperature, and pressure anomalies. Details on the data and analytical techniques are given in section 2. In section 3, we identity the annular modes in the model results and demonstrate their remarkable realism by direct comparison with observations. Section 4 summarizes the eddy properties and related forcing in both model and observations. Section

5 describes some index of refraction arguments that account for the nature of eddy propagation. Finally, a summary is given in section 6.

2. Data and analysis

The model dataset is obtained from a 100-yr control run of the Geophysical Fluid Dynamics Laboratory (GFDL) GCM with rhomboidal 30 resolution and 14 vertical ''sigma'' levels (R30L14). The GCM output is given on an approximately 3.75° lat × 2.2° long grid and has diminishing vertical resolution from the surface to the middle stratosphere. For our analysis, the sigma levels are interpolated onto 11 pressure surfaces, ranging from 1000 to 50 hPa. In the simulation analyzed here, the model's bottom boundary is specified with realistic orography and seasonally varying climatological sea surface temperature (SST). Further details on the model are given by Gordon and Stern (1982), Lau and Nath (1990), and references therein.

We also employ the 1958–98 global observational dataset from the National Centers for Environmental Prediction–National Center for Atmospheric Research (NCEP–NCAR) reanalyses (Kalnay et al. 1996). The dataset contains daily averages of geopotential height, horizontal wind, and temperature fields on a 2.5° lat × 2.5° long grid at 17 vertical pressure levels extending from 1000 to 10 hPa. The vertical velocity is given on the same horizontal grid but only at 12 levels, ranging from 1000 to 100 hPa.

The leading mode of low-frequency variability is identified by performing an empirical orthogonal function (EOF) analysis on the monthly anomalies, as explained in LH. The normalized principal component (PC) of the leading 1000-hPa geopotential height EOF serves as the index for the annular mode. The standard deviation for this leading PC in the model is about 351.4 (451.6) m in SH (NH). The standard deviation for the reanalyses is comparable to the model: 323.9 (412.0) m in SH (NH).

In the GFDL output, NAM/SAM explains about 26%/35% of the total variance in the respective domain. The fraction of explained variance decreases by about 5% in the reanalyses (Fig. 1, top). The annular mode is also well separated from higher EOF modes according to the criterion of North et al. (1982). The annual cycle of the index variance is shown in the middle panel of Fig. 1. In the SH, the variance tends to peak weakly during the late winter months, with the model result slightly larger than the reanalysis in early spring. On the other hand, the NH variance exhibits a stronger seasonal variation with largest values also occurring in the winter months. Note that the NH reanalyses variance exceeds the model during midwinter time and declines rapidly as spring arrives. A pronounced jump in the NAM index variance also appears between December and January in the reanalyses.

We note that our index differs slightly from the one used by TW and Baldwin and Dunkerton (1999). Thompson and Wallace based their NAM (SAM) index on the leading EOF of the observed monthly mean sea level pressure (850-hPa geopotential height). Baldwin and Dunkerton, who also used the NCEP–NCAR reanalyses, derived their NAM index from the leading EOF of simultaneous multilevel monthly anomaly geopotential height limited to the wintertime (December–February).

The time series of the annular mode amplitudes are statistically equivalent to red noise. Figure 1 (bottom) shows the estimated power averaged from the spectra of several 64-month segments of the leading 1000-hPa geopotential height PC (i.e., 18 and 7 realizations for the model and reanalyses, respectively). The displayed spectra thus have a bandwidth of approximately 0.016 cycles per month and at least 36 (14) degrees of freedom for the model (reanalyses) case. Using the F-test, the estimated spectra are found to be consistently below the 95% significance level at each spectral estimate, so that the time series are well modeled by a red noise process. The SAM variance in the GFDL model slightly exceeds that of the reanalyses and is slightly redder.

Composite analysis is based on the annular mode index. The high (low) phase composite consists of averages over months with index values above (below) the +1.5 (−1.5) standard deviation. In the model output of 1200 months, 75 (85) months belong in high (low) NAM phase category and 46 (93) months as the high (low) SAM phase. In 492 observed months, 29 (31) months are classified as high (low) NAM phase and 29 (33) months as high (low) SAM phase. The model results tend to have a distribution of index amplitude that is skewed toward more extreme deviations of the low phase than the high phase, especially in the SH.

3. The annular mode structure

a. Height

The SAM and NAM geopotential height anomalies at 1000, 500, and 200 hPa are shown in Fig. 2 for the GFDL model (left column) and the NCEP–NCAR reanalyses (right column). These anomalies are shown as regression maps using the convention adopted by TW. Only anomalies related to the high phase of the annular modes, defined with anomalously low heights over the polar region, are shown. The low phase structure is just opposite in sign.

In both hemispheres and in each dataset, the annular mode structures are dominated by a large degree of zonal symmetry and describe a meridional see-saw in atmospheric mass between the high latitudes and the midlatitudes. This north–south fluctuation occurs at nearly all longitudes in the SH but is limited mainly to the oceanic sectors in the NH. Relatively strong centers of action are noted over the North Atlantic. Generally, the phase structure tilts very little with altitude although

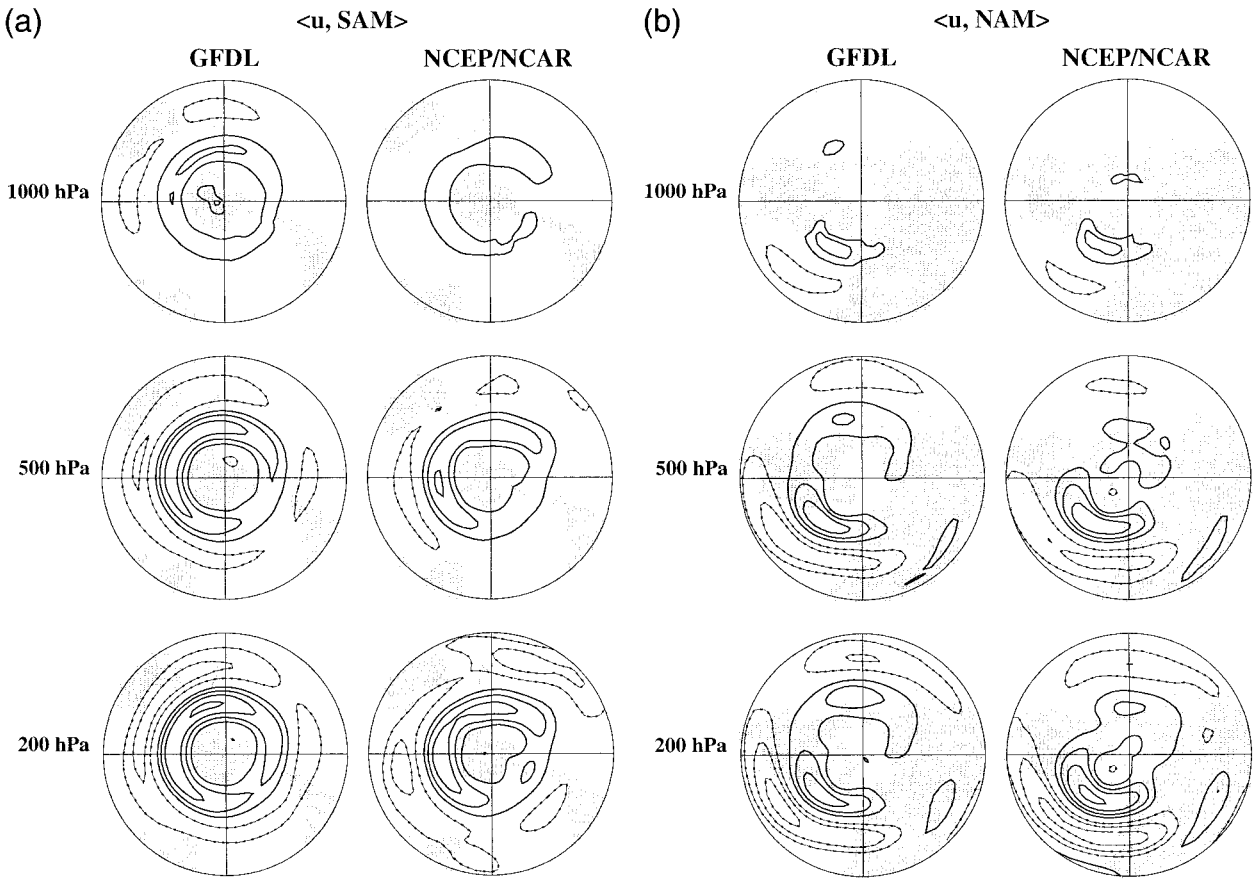

FIG. 3. (a) Zonal wind anomalies associated with SAM at three levels for the (left) GFDL model and (right) NCEP–NCAR reanalyses results. These patterns are shown as regression maps of the monthly zonal wind anomalies (u) onto the annular mode index. Negative (positive) anomalies are given by connected dash (solid) contours. The zero contour is omitted. The contour interval is 1.0 m s^{-1} per standard deviation of the index. (b) Same as Fig. 3a except for NAM.

the amplitude increases at higher levels. We note that the NAM 1000-hPa height pattern is very similar to the NAO pattern. This supports our assertion in the introduction that the NAM and the NAO are really the same phenomenon, as discussed by Wallace (2000).

In the SH, the dominant mode derived from the model appears remarkably similar to that of the observations in both structure and amplitude and bears a strong resemblance to the leading SH height EOF shown in previous studies (e.g., Rogers and van Loon 1982; Karoly 1990). Various local extrema (e.g., near New Zealand and the Ross Sea) are well captured in both datasets. In the NH, while gross features are similar between the GFDL and the reanalyses, notable differences can be found. The amplitude growth with altitude in the reanalyses exceeds the model results, particularly for the negative anomalies. As noted in LH, the negative anomaly amplitude maximum on the Siberian side of the North Pole surpasses that on the Greenland side at 200 hPa in the GFDL result. In the reanalyses, the negative anomaly amplitude is largest near Greenland (see Fig. 2b).

For both model and reanalyses, the regression maps of height anomalies at other levels below 100 hPa onto the NAM/SAM index are nearly identical to the leading EOF height pattern at each corresponding level (see the spatial correlation values in Table 1). The temporal correlation between the NAM/SAM index and the leading PC at each level also tends to be large below 100 hPa (see also Table 1). These correlation statistics suggest that the annular mode defined by the 1000-hPa height field characterizes much of the leading mode of variability in the entire troposphere.

Above 100 hPa, the correlation values fall noticeably with altitude. In general, the decline of the spatial correlation values across the tropopause is less pronounced in the reanalyses. This difference can be attributed to the poor simulation of the lower stratosphere by the GFDL model, whose vertical resolution above 200 hPa is sparse. Indeed, the leading EOF pattern for 50-hPa height in the GFDL simulation deviates markedly from the observed behavior at 50 hPa (not shown). The temporal correlation between the leading 50-hPa height PC and the SAM index is weak in the reanalyses. Such weak correlation is due to the fact that, while much height variability near the surface occurs throughout the winter

TABLE 1. Relationships of the normalized leading PCs and EOFs for the geopotential height (Z) anomalies at 500, 200, 100, and 50 hPa to indices and spatial structures of the annular modes for the GFDL model output and the NCEP–NCAR reanalyses. Here, ⟨NAM, X⟩, e.g., denotes the spatial pattern derived by regressing Z anomalies at X hPa onto the NAM index.

			GFDL			
	Variance exp. (%)		Temporal correlation with		Spatial correlation with	
EOF/PC	SH	NH	SAM index	NAM index	⟨SAM, X⟩	⟨NAM, X⟩
Z_{500}	32	22	0.97	0.93	0.99	0.99
Z_{200}	29	21	0.94	0.87	0.99	0.99
Z_{100}	28	24	0.88	0.67	0.99	0.95
Z_{50}	28	33	0.56	0.21	0.87	0.65
			NCEP–NCAR			
	Variance exp. (%)		Temporal correlation with		Spatial correlation with	
EOF/PC	SH	NH	SAM index	NAM index	⟨SAM, X⟩	⟨NAM, X⟩
Z_{500}	26	17	0.93	0.88	0.99	0.96
Z_{200}	24	18	0.80	0.82	0.99	0.97
Z_{100}	36	32	0.60	0.68	0.87	0.99
Z_{50}	33	44	0.20	0.55	0.86	0.98

months (May–October; Fig. 1, middle), fluctuations at 50 hPa are mainly concentrated in late Spring when the stratospheric polar vortex breaks down (as illustrated by TW). Again, the observed stratospheric variability is not well simulated in the 14-level GFDL model. We emphasize that the GFDL model employed in this study was not intended to properly resolve the stratosphere. Nonetheless, much of the observed tropospheric height variability is realistically generated in the model.

b. Zonal wind

Figure 3 shows the zonal wind anomalies associated with the high phase of annular modes for the GFDL output and the NCEP–NCAR reanalyses. As with the height field, the zonal wind regression patterns exhibit a nearly equivalent barotropic structure extending from the surface to the lower stratosphere. The wind anomaly structure generally describes the north–south displacement of the midlatitude jet.

In the SH, the jet displacement appears at almost all longitudes although a stronger jet displacement occurs on the Australian side of the Antarctic than on the South American side. This asymmetry is present in both the simulation and the reanalyses. In the NH, the jet displacement appears mainly over the oceanic sectors and most strongly over the North Atlantic at all levels. Thus, the global NAM pattern appears much more zonally asymmetric than the SAM patterns. Over the North Pacific, relatively weaker wind fluctuations appear more prominent in the GFDL model, which exhibits larger low height anomalies near Siberia (noted in Fig. 2b). Consequently, the model NH patterns appear more zonally symmetric than in the reanalyses.

Figure 4 illustrates the composite zonal mean zonal wind ($\overline{u}$) structures for high and low composites of the annular mode index (top and middle rows). In both hemispheres, the observed composites reveal a subtropical jet core centered around 30° and 200 hPa. In the GFDL SAM wind composite, this subtropical jet core is displaced poleward by 5°–10°. While the NH subtropical jet core is situated similarly in the composites of both datasets, the simulated structure is considerably weaker than the observed structure. In all cases, a midlatitude jet is evident around 40°–60°.

Despite these notable differences in the subtropical jet structure, composite differences (high minus low) in both datasets are remarkably similar (Fig. 4, last row). This may indicate that the SAM and NAM modes of variability are not sensitive to subtropical jet structure but rather are an interaction of the eddy-driven surface midlatitude winds. Recent work on the interaction of baroclinic eddies with zonal wind suggests that eddy, mean flow interactions are most sensitive to low-level winds (Balasubramanian and Garner 1997; Hartmann 2000). The difference patterns unveil a strong midlatitude anomalous wind dipole structure centered near 40°–60°S for SAM and 35°–55°N for NAM throughout the troposphere (Fig. 4, bottom). These patterns generally reflect stronger midlatitude westerly wind poleward (equatorward) of 45° during the high (low) phase. Consistent with Fig. 3, the composite zonal wind differences show a nearly equivalent barotropic vacillation of wind anomalies. In the SH, this vacillating pattern emerges mainly below 100 hPa. In the NH, the pattern extends well into the lower stratosphere in the reanalyses.

The SAM composite wind difference reveals westerly anomalies extending well in the lower stratosphere in both the reanalyses and the model (Fig. 4a). However, the anomalous wind structure obtained by regressing monthly wind anomalies onto the SAM index decays with altitude above the tropopause (see Fig. 2 of LH; see also TW). Composite techniques that average all ''extreme'' SAM events appear to capture strong non-

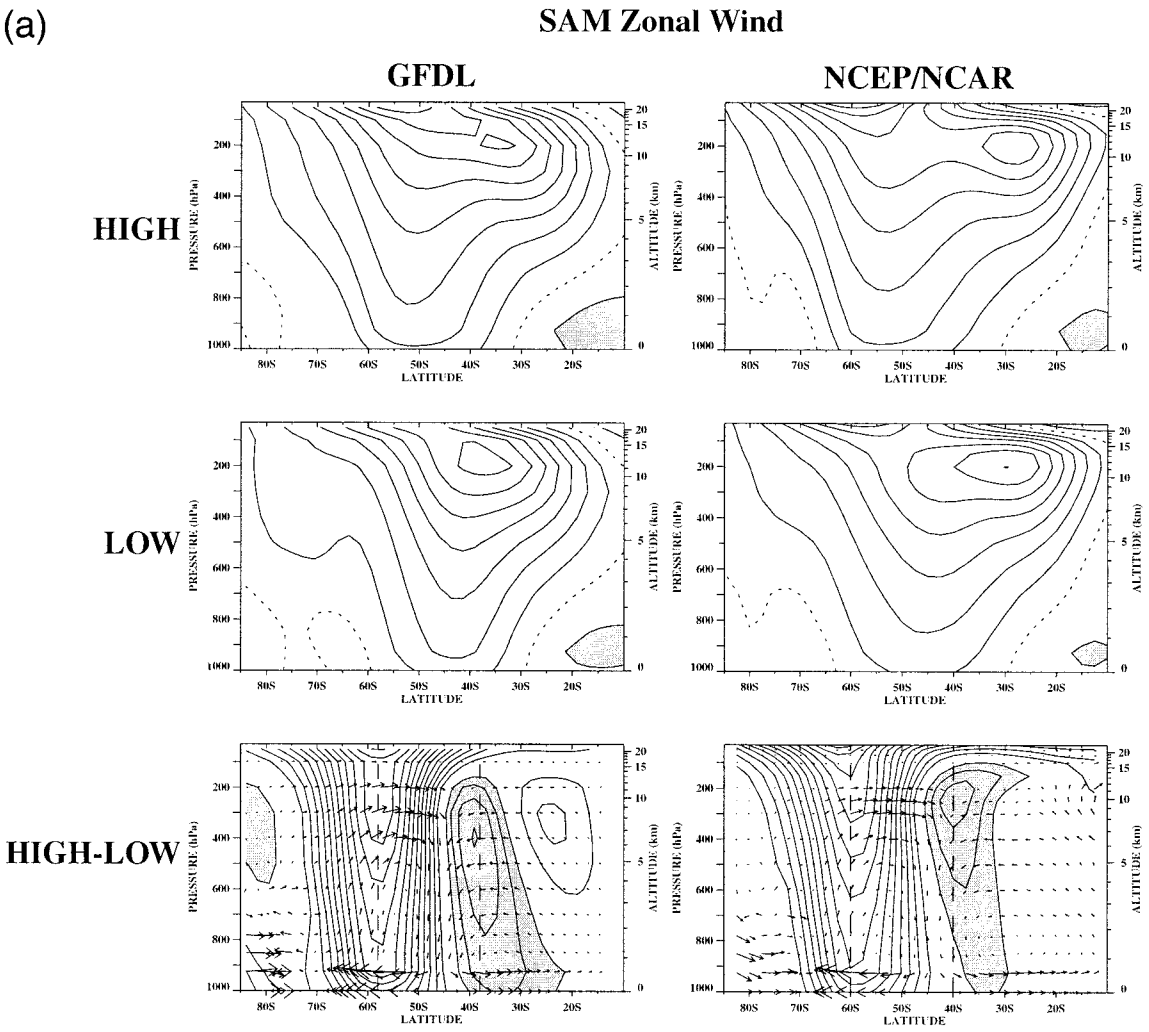

FIG. 4. (a) SAM zonal mean zonal wind composites for the (left) GFDL model and the (right) NCEP–NCAR reanalyses results: (top) high phase composite, (middle) low phase composite, and (bottom) their difference. Contour interval is 5 m s^{-1} for the composites and 1 m s^{-1} for their difference. Negative values are shaded; zero contour is given by the dotted line. Composite difference of the meridional circulation is superimposed in the bottom panel as vectors. The longest vector is about 0.75 m s^{-1}. The dipole centers of the composite zonal wind difference are approximated by the vertical dashed lines.

linear features that manifest themselves in the lower stratosphere.

The anomalous meridional circulation is generally similar in both datasets (see arrows in Fig. 4, bottom) and describes the modulation of the Ferrel circulation. As noted by LH and TW, the strongest anomalous sinking motion appears around the node of the dipole structure in anomalous zonal wind. Near the surface, strong anomalous meridional winds diverge away from 45° lat, and the associated Coriolis acceleration balances the effect of surface friction on the anomalous zonal winds. In the upper troposphere, strong anomalous meridional winds converge toward 45° lat, and the associated Coriolis acceleration is balanced by eddy momentum flux convergence. Thus, eddy momentum fluxes in the upper troposphere appear to be important in maintaining the wind anomalies aloft, and in maintaining the mean meridional circulation that supports the surface wind anomalies against friction (Hartmann and Lo 1998). We explore the role of eddy forcing in the next section.

4. Zonal-mean eddy forcing and propagation

We compute composites of the eddy forcing of momentum using the Eliassen–Palm (EP) flux divergence (Edmon et al. 1980; Andrews et al. 1987). Forcing due to meridional divergence of eddy momentum fluxes (''barotropic'' forcing) and vertical divergence of eddy heat fluxes (''baroclinic'' forcing) make up the EP flux divergence (e.g., Hartmann and Lo 1998). The eddies can be divided into stationary waves, defined as zonal asymmetries in the monthly means, and transient waves, defined as the deviations from the monthly means. The

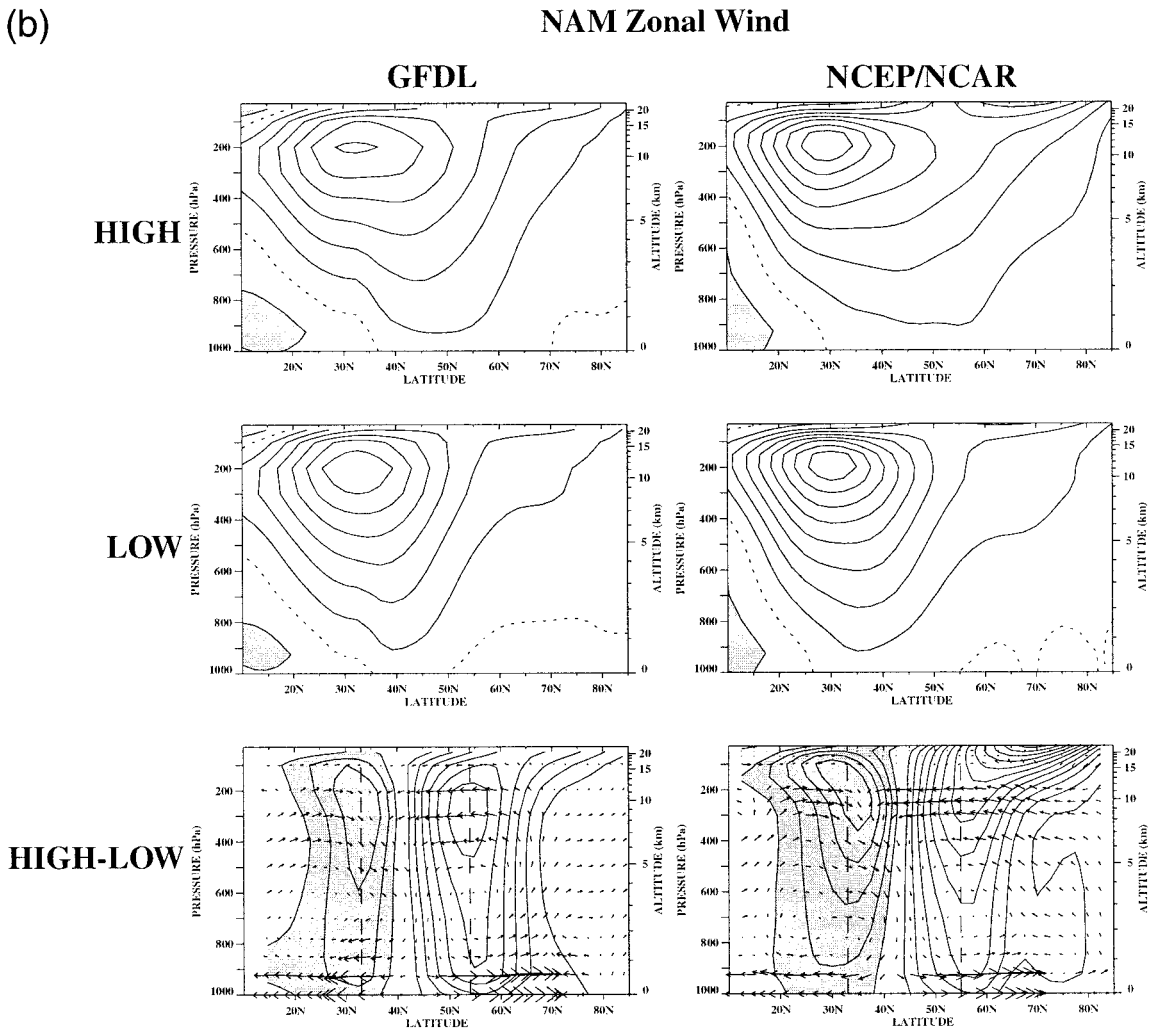

FIG. 4. (b) Same as (a) except for the NAM composites.

total eddy forcing includes both stationary wave and transient wave contributions.

The meridional cross sections of the anomalous eddy barotropic forcing are illustrated in the top panels of Fig. 5. The prevailing structure of the momentum flux convergence is a midlatitude dipole located near 300 hPa, which indicates a relatively stronger poleward eddy momentum flux across 45° lat during the high phase of the NAM and SAM. In the SH, the high-latitude forcing anomaly in the GFDL result exceeds that of the reanalyses.

The centers of the anomalous barotropic forcing dipole nearly coincide with the latitude of the zonal wind anomalies shown in Fig. 4 (bottom). For convenience, the dipole centers of the zonal wind anomalies are shown as vertical dashed lines in Fig. 5. As discussed in section 3, forcing by the eddy momentum fluxes appears to maintain the wind anomalies in the upper troposphere and balance the Coriolis torques associated with the anomalous mean meridional circulation (see also Fig. 6, bottom).

The properties of the barotropic eddy forcing can be summarized by vertically averaging the forcing between 700 and 100 hPa. The solid line in middle panels of Fig. 5 displays the resulting meridional profile. We chose not to extend the averaging process down to 1000 hPa to avoid the strong forcing dipole near the surface at 35°N in the GFDL result. This dipole pattern is apparently a spurious result of our interpolation from sigma to pressure surfaces in the region of the Himalayas (Fig. 5b, upper left).

Decomposing the anomalous barotropic eddy forcing profile into its stationary and transient components reveals that the forcing is partitioned similarly in both datasets but differently in each hemisphere (see dotted and dashed lines in Fig. 5, middle). In the SH, barotropic forcing by the transients dominates over the stationary wave contribution; the transient forcing profile is nearly

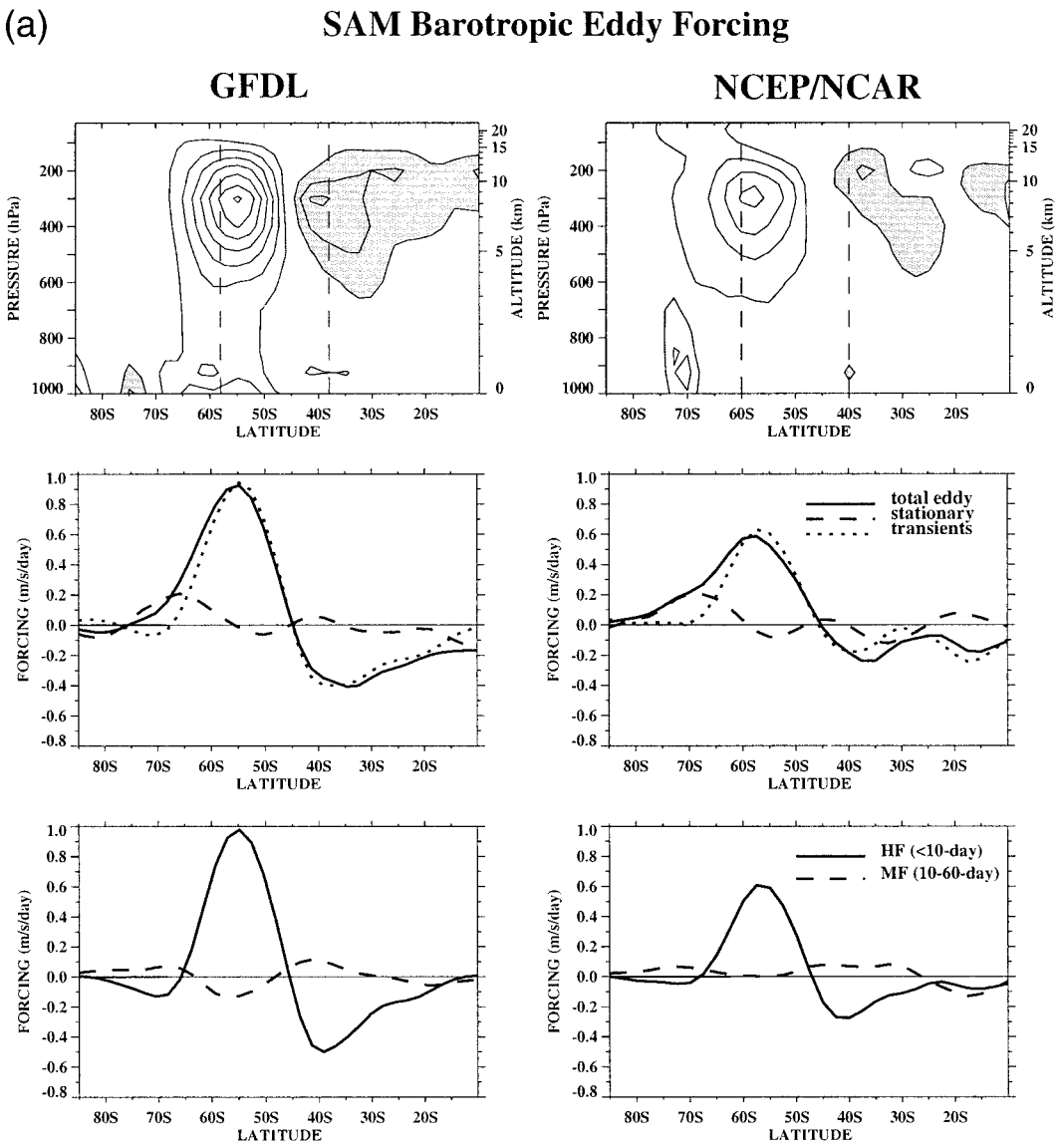

FIG. 5. (a) (top) SAM composite difference of the forcing due to eddy momentum flux divergence. Easterly acceleration is shaded. Contour interval is 0.25 m s^{-1} day^{-1}; zero contour is omitted. Vertical dashed lines roughly mark the dipole centers of the zonal wind anomalies shown in Fig. 4. (middle) Vertically averaged (700–100 hPa) forcing due to eddy momentum flux divergence (solid line). Contributions from stationary wave and transient components are overlaid. (bottom) Decomposition of the transient part into the high-frequency (HF; <10 day) and middle frequency (MF; 10–60 day) parts.

identical to the total barotropic eddy forcing profile. The stationary wave forcing is largest around 70°S. In the NH, the stationary wave contribution accounts for a considerable fraction of the anomalous wind acceleration. The strongest stationary wave forcing is found around 60°N. Transient eddy forcing also makes an important contribution, particularly equatorward of 45°N. The relative importance of eddy forcing due to stationary waves and transient eddy in the NH is consistent with the results of DN.

The bottom panels of Fig. 5 show the separation of the transient barotropic forcing into its high-frequency (<10 day) and middle-frequency (10–60 day) parts. Clearly, high-frequency transients associated with synoptic waves govern much of the total transient forcing. Middle-frequency forcing can be sizeable (especially in NH), and its presence tends to oppose the effects of the high-frequency transients.

Composites of the total eddy forcing (barotropic and baroclinic components) are demonstrated in Fig. 6 (top two rows). The total eddy forcing composites (contours) appear similar between both datasets. However, the eddy forcing amplitude in the GFDL results consistently exceeds that in the reanalyses. In both hemispheres, the

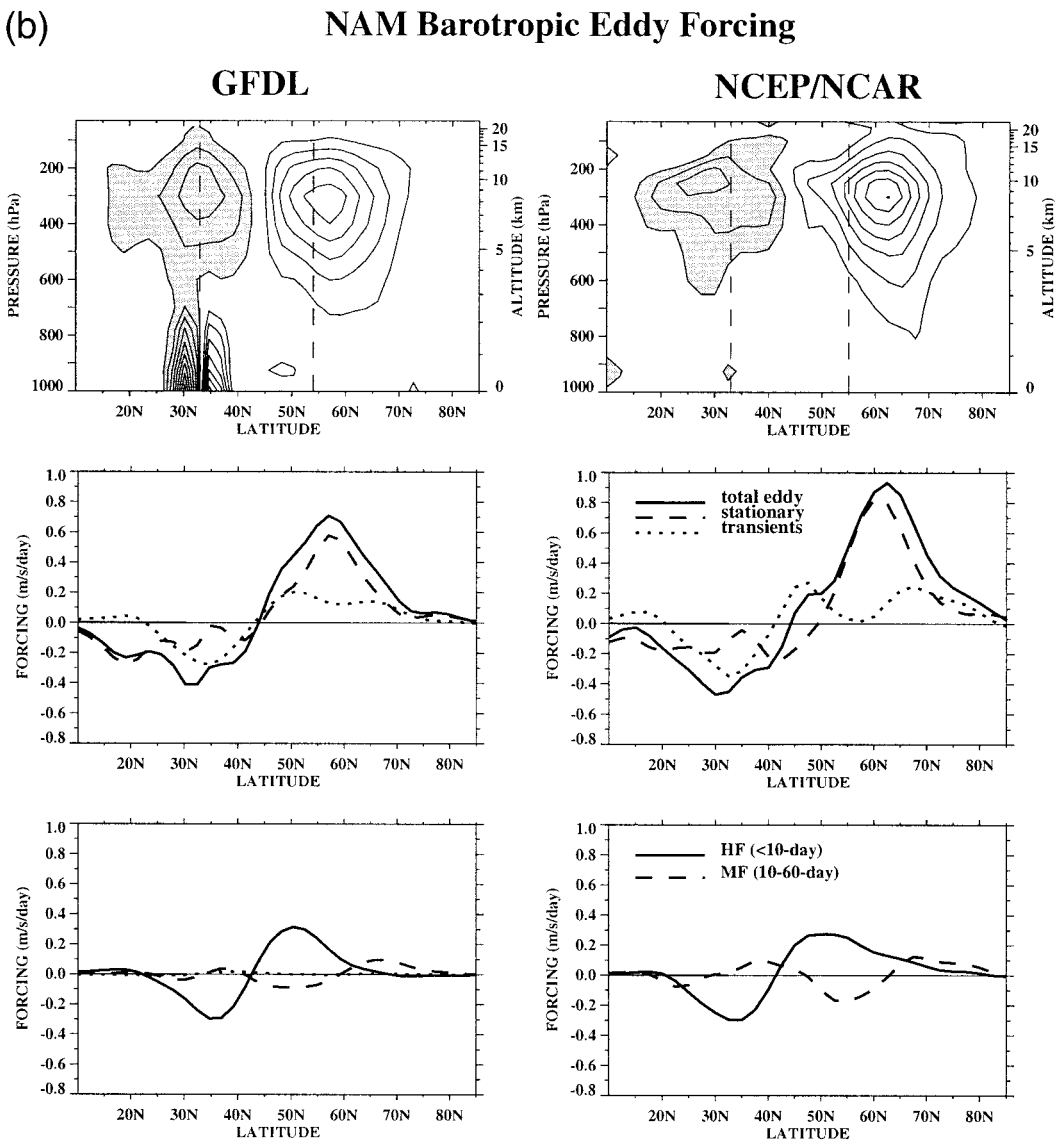

FIG. 5. (b) Same as (a) except for the NAM composite difference.

eddy forcing due to converging EP fluxes (negative contours) in the middle to upper troposphere around 50°–60° is generally stronger during the low phase.

Comparing the top rows of Fig. 5 with the third row of Fig. 6 yields insights into the role of eddy heat fluxes associated with the baroclinic eddy forcing component. With the exception of the observed SAM result (Fig. 6a, third row, right column), the anomalous total eddy forcing structure embodies much of the barotropic forcing shown in Fig. 5 (top row). This similarity attests to the importance of eddy momentum fluxes in the upper troposphere. Nonetheless, at these levels, baroclinic effects can enhance the anomalous easterly acceleration near 35°. The baroclinic contribution is generally largest below 300 hPa and accounts for the vertical tilt in the structure of the total anomalous eddy forcing. Above 200 hPa, its effects can lead to strong westerly forcing in the high-latitude middle stratosphere (e.g., Fig. 6b, third row, right column). The inclusion of the baroclinic forcing component also tends to better align the centers of the anomalous eddy forcing with the dipole centers of the zonal wind anomalies in the upper troposphere (compare third row of Fig. 6 with top row of Fig. 5).

In the reanalyses momentum budget for SAM (Fig. 6a, third row, right column), the westerly acceleration center of the barotropic forcing near 300 hPa is washed out by the baroclinic term. Consequently, the difference pattern at 300 hPa differs markedly from the difference pattern for barotropic forcing. Nonetheless, the overall difference pattern in the upper troposphere is still qualitatively similar to the simulated SAM results.

The latitudinal positions of the anomalous total eddy

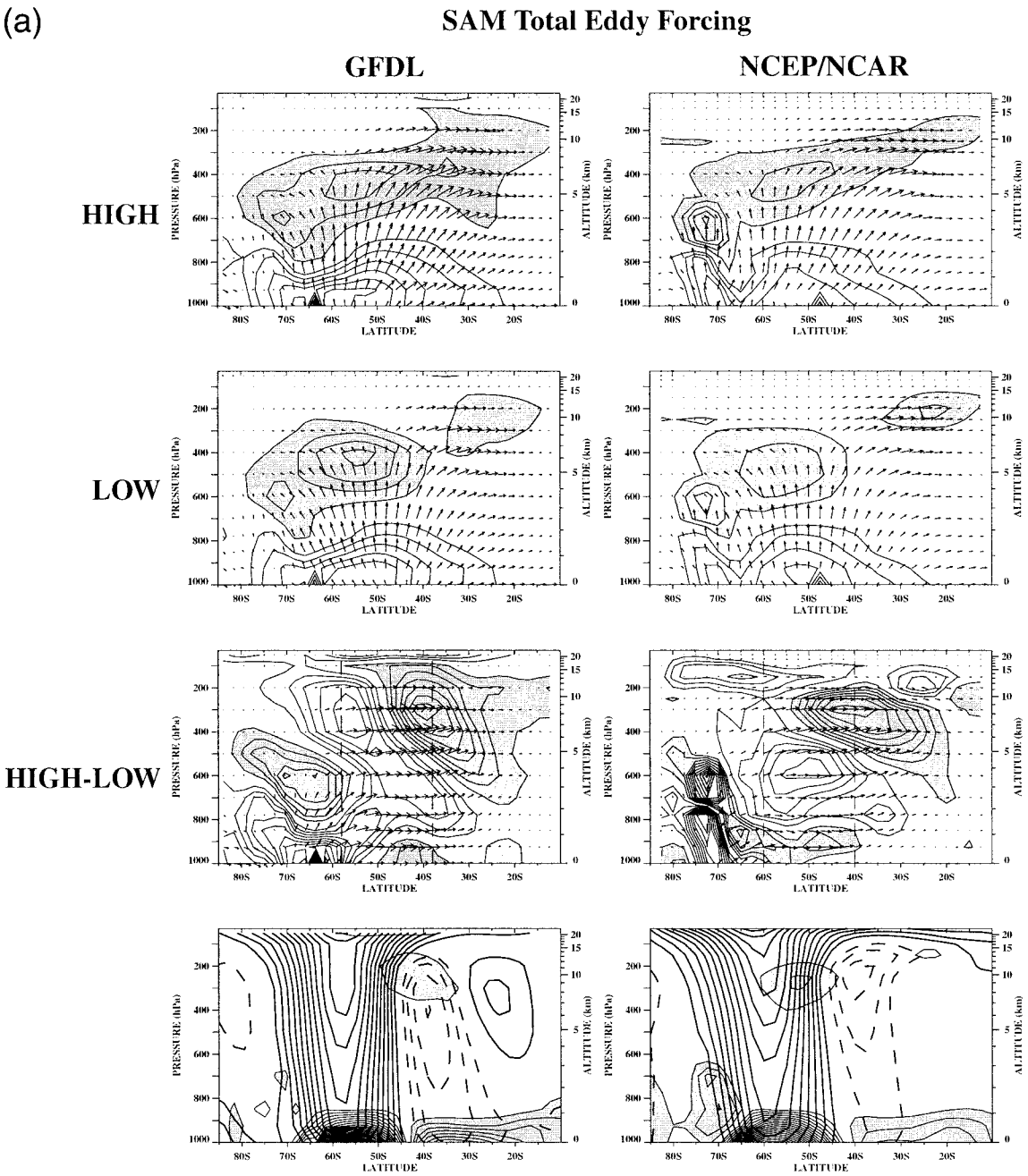

FIG. 6. (a) SAM composites of the total eddy forcing and their difference. Contour interval for the composites (their difference) is 1.5 (0.25) m s^{-1} day^{-1}. Negative values (denoting easterly acceleration) are shaded and zero contour is omitted. Eliassen–Palm flux vectors (divided by the background density) are superimposed on the plots. The longest composite vector is 1.4×10^8 m^3 s^{-2}. Vertical dashed lines roughly mark the dipole centers of the zonal wind anomalies shown in Fig. 4. (bottom) Composite difference of the sum of the total eddy forcing and Coriolis forcing due to mean meridional circulation (thin contour). Composite difference of the zonal wind anomalies shown in Fig. 4 (bottom) is repeated in thick contours.

forcing centers tend to align with the zonal wind anomalies shown in Fig. 4 above 500 hPa. This correspondence underlines the importance of eddies in maintaining the wind anomalies in the upper troposphere. In addition, the sum of the anomalous total eddy forcing and the Coriolis forcing due to anomalous mean meridional circulation is small everywhere except near the surface (see Fig. 6, bottom), further illustrating the importance of the associated anomalous mean meridional circulation in sustaining the surface wind anomalies against friction (as noted in Fig. 4, bottom). These connections have been discussed previously by Yu and

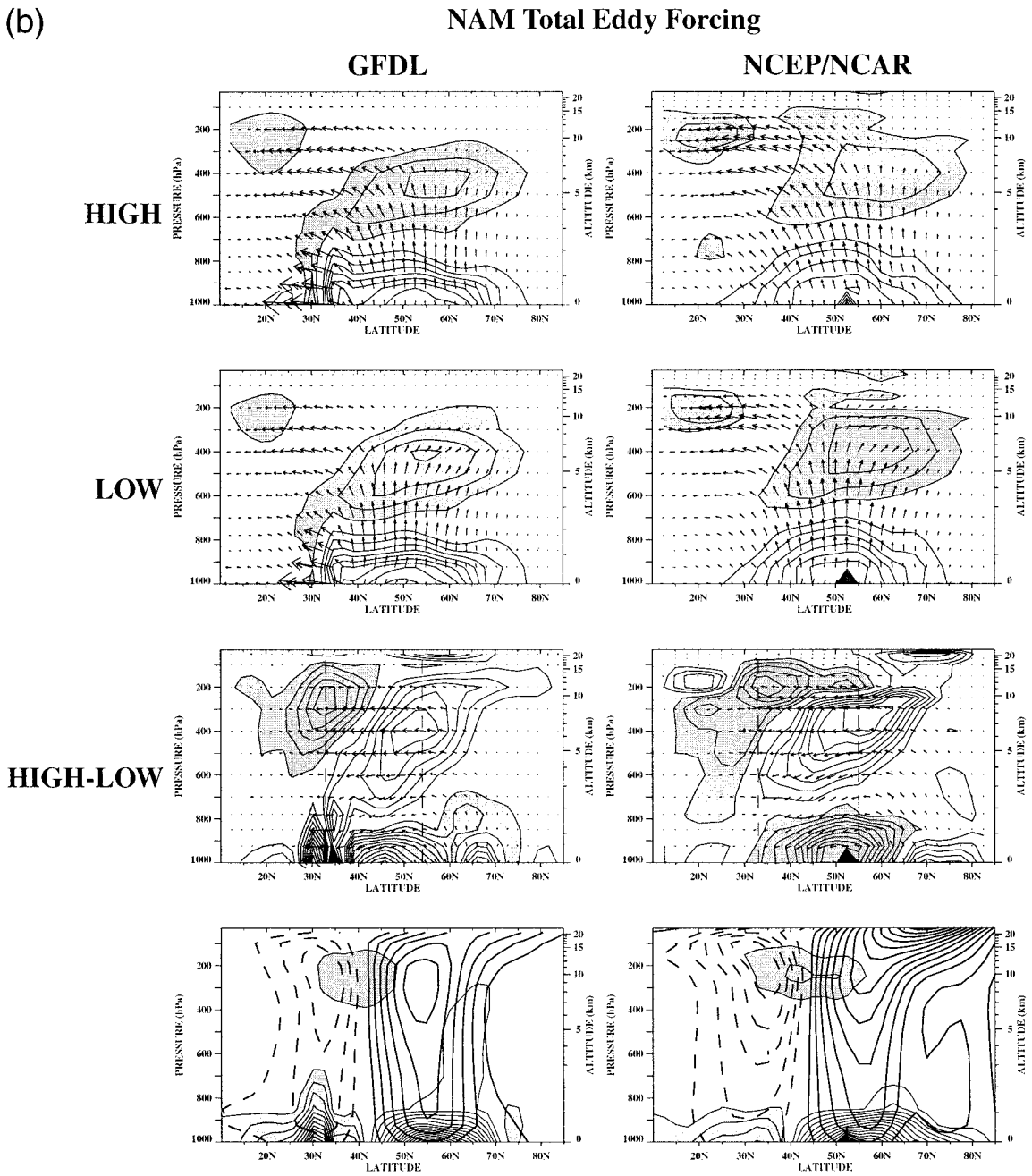

FIG. 6. (b) Same as (a) except for the NAM composites. The longest composite vector is 4.9×10^8 m^3 s^{-2}.

Hartmann (1993) and Hartmann and Lo (1998) in the SH and by DN in the NH.

The arrows in Fig. 6 represent the EP flux vectors, which approximate the direction of wave energy propagation. The EP flux vectors in the GFDL composites largely parallel those in the reanalyses. In both hemispheres, the wave activity emanating from the lower boundary tends to propagate equatorward upon reaching the tropopause. Equatorward propagation is stronger during the high phase since a significant amount of energy during the low phase tends to veer poleward. Differences between low and high phases are present at all levels but are most obvious between 600 and 200 hPa. The difference arrows mainly point equatorward, indicating anomalous poleward eddy momentum flux in the high phase.

As shown in Fig. 4, the difference plots of the zonal mean zonal wind NAM and SAM composites appear quite similar. Both describe the meridional shift of the jet throughout the troposphere although the SAM struc-

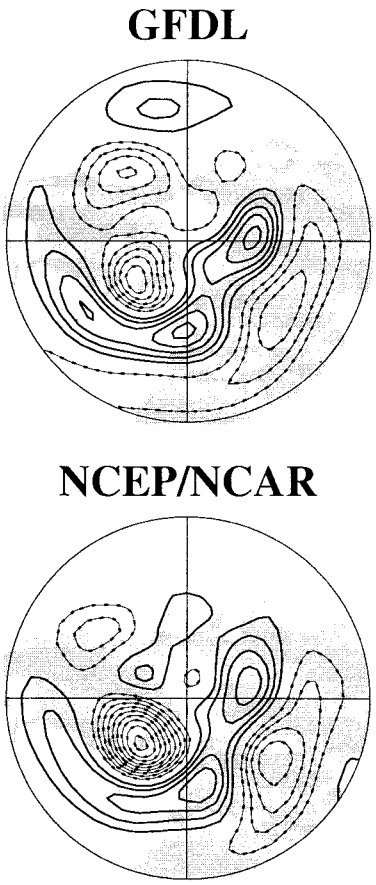

FIG. 7. The 500-hPa composite difference of the geopotential height stationary wave. Contour interval is 20 m. Zero contour is omitted. Negative values are shown by connected dashed contour.

ture is centered slightly more poleward. Our results in Fig. 5 demonstrate that the maintenance of zonally symmetric anomalous wind structures are however dominated by different types of eddies in each hemisphere. This difference reflects the contrast in land–sea distribution between the NH and SH. Thus, while the zonally symmetric components of the NAM and SAM appear alike, they are fundamentally different.

The NAM composite difference of the stationary wave pattern is shown in Fig. 7 for the model and the reanalyses. Notable differences are found over the oceanic sectors. The model results have a more pronounced fluctuation over the North Pacific while the reanalyses results show stronger changes over the North Atlantic. Regardless of the these differences, the overall structures are remarkably similar in both datasets despite the absence of anomalous SST in the model. These patterns are also in good agreement with the anomalous stationary wave responses to midlatitude $\overline{u}$ variations between 35°N and 55°N shown by Ting et al. (1996, see their Fig. 6a).

In agreement with DN, our study suggests that these anomalous stationary wave patterns along with the associated anomalous synoptic waves act to support the zonal flow anomalies characterized by NAM. As shown in LH for the GFDL results (see their Fig. 3), global patterns of anomalous NH stationary and synoptic wave activity indicate synergetic eddy momentum forcing mainly over the oceanic sector in support of the NAM zonal wind anomalies shown in Fig. 3b. On the other hand, Ting et al. (1996) and DeWeaver and Nigam (2000b) suggest these stationary wave patterns may also be maintained to some extent by the midlatitude jet fluctuation through zonal-eddy coupling. Thus, a two-way, reciprocal relationship (i.e., positive feedback interaction) between the stationary waves and zonal wind anomalies may be at work, as perhaps first suggested by Kodera et al. (1991) and recently by DeWeaver and Nigam (2000b).

5. Index of refraction arguments

We attempt to account for the wave energy propagation in NH with the quasigeostrophic refractive index (n^2) as given in Chen and Robinson (1992):

$$n^2 = \frac{\overline{q}_\varphi}{\overline{u} - (a\sigma\cos\varphi)/s} - \left(\frac{s}{a\cos\varphi}\right)^2 - \left(\frac{f}{2NH}\right)^2, \quad (5.1)$$

where

$$\overline{q}_\varphi = \frac{2\Omega}{a}\cos\varphi - \frac{1}{a^2}\left[\frac{(\overline{u}\cos\varphi)_\varphi}{\cos\varphi}\right]_\varphi - \frac{f^2}{\rho_0}\left(\rho_0\frac{\overline{u}_z}{N^2}\right)_z. \quad (5.2)$$

Here, s is the zonal wavenumber, σ is the wave frequency (radian per second), N^2 is the buoyancy frequency, H is the scale height (7 km), f is the Coriolis parameter, a and Ω are the earth's radius and angular frequency, ρ_0 is the background density, and φ is latitude. Theoretically, the wave activity can propagate in regions of positive refractive index and avoid negative values (Andrews et al. 1987). In addition, the wave activity tends to be refracted toward large positive index values.

Figure 8 shows the NAM refractive indices for the largest stationary wave (zonal wavenumber 1). Recall that, in the NH, anomalous eddy momentum forcing is mainly due to stationary waves (e.g., Fig. 5b). The most prominent characteristic of the refractive index is the local maximum situated in the high latitudes just below the tropopause. According to WKBJ theory (Andrews et al. 1987), this index of refraction maximum should tend to attract waves toward the polar region, giving rise to equatorward momentum fluxes. During the low phase of the annular mode, this index of refraction maximum is considerably stronger than during the high phase, as evident by the large negative regions near 65°N in the composite difference (bottom row of Fig. 8).

Analogous variation in stationary wave energy propagation in relation to the anomalous shifting of the background jet (and associated index of refraction) was mod-

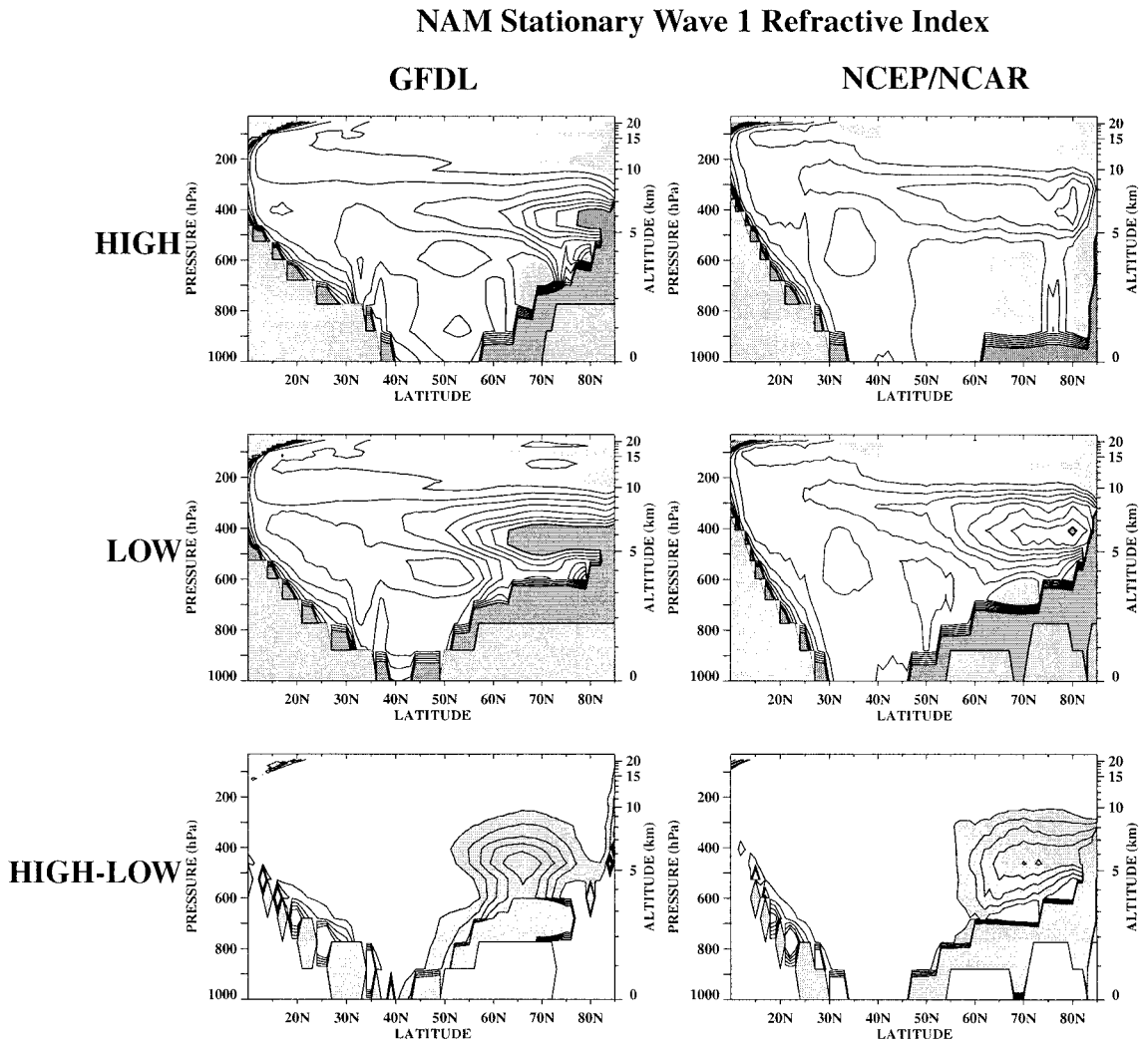

FIG. 8. NAM composites and their difference of the nondimensionalized quasigeostrophic refractive index (a^2n^2) for zonal wavenumber 1 stationary wave. Contour intervals for the composites (differences) are 50 (40). Negative values are lightly shaded. Heavily shaded area represents region where the refractive index is greater or equal to 400.

eled by Nigam and Lindzen (1989). They demonstrated that slight equatorward displacement of the subtropical jet (somewhat like the equatorward jet displacement during the low NAM phase) produces increased stationary wave propagation into higher latitudes of the troposphere and lower stratosphere (see their Fig. 16). However, the anomalous dipole structure of the wind perturbations in their study had a node that is about 10° closer to the equator than the dipole structure of the NAM (see bottom of Fig. 4b).

Detailed examination shows that the anomalous local maximum structure in the refractive index shown at the bottom of Fig. 8 is most sensitive to the term related to vertical zonal wind shear. Excluding both the second and third terms in the right-hand side (rhs) of (5.2) does not yield the negative extrema near 6 km in the composite difference pattern shown in Fig. 8. Exclusion of the third term in the rhs of (5.1) also fails to generate the local negative extrema. We find that the third term in the rhs of (5.2) accounts for most of the difference in n^2 between the high and low phases. Expansion of this third term into $(f^2/\rho_0)(\rho_0/N^2)_z\overline{u}_z$ and $(f^2/\rho_0)(\rho_0/N^2)\overline{u}_{zz}$ reveals that the former quantity, which is related to the vertical wind shear, is most important.

As displayed in Fig. 4, the zonal flow during the high phase of the annular mode exhibits considerably stronger westerly winds and westerly vertical wind shear (i.e., zonal wind increasing with altitude) than the low phase between 60° and 80°N. The stronger westerly winds during the high phase cause waves to be less strongly refracted toward the pole, resulting in anomalous equatorward wave propagation and poleward momentum anomalies. The poleward momentum anomalies in turn support the high-latitude westerlies. In the model, high-latitude vertical wind variation is generally much weaker than observation in both high and low phases. Con-

sequently, high-latitude regions of very large refractive index values (heavily shaded) are found in both phases of the model results.

The numerical study of Chen and Robinson (1992) found that strong vertical wind shear also impedes the vertical propagation of planetary waves across the tropopause. One might reasonably speculate that during the high phase, propagation of planetary waves into the stratosphere would be inhibited relative to the low phase. Since planetary waves tend to break in the stratosphere upon reaching their critical surfaces and weaken the polar vortex, one would expect that the polar vortex will be stronger when the tropospheric annular mode is in its positive phase. When the tropospheric jet is displaced equatorward in the low phase, one would expect more planetary wave activity in the stratosphere and a weaker polar vortex. These associations between tropospheric annular variability and stratospheric variability are essentially what has been described by Baldwin and Dunkerton (1999) and TW and occur both in month-to-month variability and in decadal trends.

6. Summary

The annular modes are identified in a 100-yr control run of the GFDL GCM as the leading modes of tropospheric month-to-month variability. In this simulation, the model's lower boundary is prescribed only with realistic topography and seasonally varying climatological SST. The simulated annular modes are shown to be very similar to those found in the NCEP–NCAR reanalyses, which includes the influence of SST interannual variability. Similarities between the model and reanalyses results confirm that the annular modes can therefore be produced entirely by internal atmospheric dynamical processes.

The characteristics of the annular modes presented here are very similar to those of recent studies by Baldwin and Dunkerton (1999) and TW who employed slightly different annular mode indices. Throughout the entire troposphere, the mode is dominated by a near zonally symmetric, meridional displacement of the jet as the polar vortex expands and contracts. The NAM spatial structure is nearly identical to the widely known NAO and, to this end, we consider them to be one and the same phenomenon (Wallace 2000). While the NAM features are dominated by a higher degree of zonal variations, the zonally symmetric components of the NAM and SAM are remarkably similar. The annular mode zonal mean zonal wind anomalous structure describes the meridional translation of the jet and associated expansion/contraction of the vortex. Strongest mode variance occurs during the cold months. This seasonal variation is very pronounced in the NH.

From composites based on the annular mode index, anomalous eddy forcing appears to maintain the zonal mean zonal wind anomalies associated with the annular modes in both model and reanalyses. Anomalous divergence of eddy momentum fluxes plays a large role in sustaining the wind anomalies in the upper troposphere while the Coriolis acceleration associated with anomalous mean meridional circulation sustains the near-surface wind anomalies against frictional dissipation. The anomalous eddy forcing reflects differences in the pattern of eddy propagation in the upper troposphere during the extreme phases of the annular mode. In the high phase, eddy energy propagates almost exclusively equatorward at these altitudes. Weaker equatorward propagation is evident during the low phase.

The type of eddy most responsible for the changed momentum fluxes that sustain the zonally symmetric component of the annular modes is different in the Southern and Northern Hemispheres. In the SH, high-frequency (synoptic) transients are mostly responsible for the wind anomalies, in agreement with past studies on SH flow vacillation (e.g., Hartman and Lo 1998; Karoly 1990). In the NH, eddy forcing due to stationary waves is most important, particularly around 60°N and in the Atlantic sector. High-frequency transients also make important contribution to the maintenance of the wind anomalies in the NH equatorward of 45°N. Thus, although the zonally symmetric component of the NAM and SAM are remarkably similar, they are fundamentally different as they are mostly maintained by different types of eddies. This difference ultimately reflects the contrasting land–sea distribution in the two hemispheres.

A first-order understanding of the interaction between NAM and stationary wave propagation can be derived from WKBJ theory relating the background wind with wave refractive properties. In the high phase, planetary Rossby waves are less strongly refracted toward the pole, so that they mainly propagate equatorward. This equatorward propagation is associated with poleward momentum fluxes, which help to sustain the poleward displacement of tropospheric westerlies associated with the high NAM phase. In the low phase, stationary waves are more strongly attracted toward the polar regions, yielding an anomalous equatorward momentum flux. The increased refractive index values in high latitudes that attract planetary waves poleward in the low index case are associated primarily with weaker vertical wind shear in the high-latitude upper troposphere during the low phase.

The planetary wave propagation characteristics can be used to link changes in the tropospheric annular mode to changes in the strength of the stratospheric polar vortex during winter. Planetary waves are strongly attracted to polar regions during the low phase of the annular mode when the tropospheric westerlies are displaced equatorward. We should expect a weaker stratospheric polar vortex then, since planetary waves weaken the polar vortex by generating irreversible mixing. This association of low NAM phase with a weakened wintertime stratospheric vortex is indeed observed. Recently, Baldwin and Dunkerton (1999) and Hartmann et al. (2000) illustrate that major stratospheric warming occurs almost exclusively during the low NAM phase due to the increased station-

ary wave activity in the lower stratosphere. When the tropospheric midlatitude westerlies are displaced toward the pole, planetary waves are refracted equatorward, less planetary wave activity propagates upward at high latitudes, and we should expect the stratospheric vortex to be stronger.

Finally, we reiterate that our composite results are based on an index derived from monthly EOF analysis. In the NH, composites computed using all months with extreme index values (exceeding ± 1.5 standard deviation) are found to be very similar to composites in which only the winter months (December–March) are employed. This is because extreme NAM index values are mostly found during the winter season as suggested by Fig. 1 (middle). We did not perform EOF analysis based only on the winter months. We expect the composites based on the analysis of the winter data would be similar to the results presented here, however.

Acknowledgments. This research was supported by the NOAA/GFDL Universities Consortium grant (Joint Institute for the Study of the Atmosphere and Ocean contribution number 703). The authors thank Drs. J. M. Wallace and C. B. Leovy and our colleagues in the consortium for their interests and helpful discussions. Mary Jo Nath at GFDL and Marc Michelsen are also acknowledged for their computing assistance. The comments of Dr. Sumant Nigam and an anonymous reviewer contributed significantly to the improvement of the original manuscript.

REFERENCES

Andrews, D. G., J. R. Holton, and C. B. Leovy, 1987: *Middle Atmosphere Dynamics.* Academic Press, 498 pp.

Balasubramanian, G., and S. T. Garner, 1997: The role of momentum fluxes in shaping the life cycles of a baroclinic wave. *J. Atmos. Sci.,* **54,** 510–533.

Baldwin, M. P., and T. J. Dunkerton, 1999: Propagation of the arctic oscillation from the stratosphere to the troposphere. *J. Geophys. Res.,* **104,** 30 937–30 946.

Chen, P., and W. A. Robinson, 1992: Propagation of planetary waves between the troposphere and stratosphere. *J. Atmos. Sci.,* **49,** 2533–2545.

DeWeaver, E., and S. Nigam, 2000a: Do stationary waves drive the zonal-mean jet anomalies of the northern winter? *J. Climate,* **13,** 2160–2176.

——, and ——, 2000b: Zonal-eddy dynamics of the North Atlantic Oscillation. *J. Climate,* **13,** 3893–3914.

Edmon, H. J., Jr., B. J. Hoskins, and M. E. McIntyre, 1980: Eliassen–Palm cross sections for the troposphere. *J. Atmos. Sci.,* **37,** 2600–2616.

Gordon, C. T., and W. F. Stern, 1982: A description of the GFDL global spectral model. *Mon. Wea. Rev.,* **110,** 625–644.

Hartmann, D. L., 1995: A PV view of zonal flow vacillation. *J. Atmos. Sci.,* **52,** 2561–2576.

——, 2000: The key role of lower-level meridional shear in baroclinic wave life cycles. *J. Atmos. Sci.,* **57,** 389–401.

——, and F. Lo, 1998: Wave-driven zonal flow vacillation in the Southern Hemisphere. *J. Atmos. Sci.,* **55,** 1303–1315.

——, J. M. Wallace, V. Limpasuvan, D. W. J. Thompson, and J. R. Holton, 2000: Can ozone depletion and global warming interact to produce rapid climate change? *Proc. Natl. Acad. Sci.,* **92,** 1412–1417.

Hoerling, M. P., M. Ting, and A. Kumar, 1995: Zonal flow-stationary wave relationship during El Niño: Implications for seasonal forecasting. *J. Climate,* **8,** 1838–1852.

Hurrell, J. W., 1995: Decadal trends in the North Atlantic oscillation: Regional temperatures and precipitation. *Science,* **269,** 676–679.

Kalnay, E., and Coauthors, 1996: The NCEP/NCAR 40-Year Reanalysis Project. *Bull. Amer. Meteor. Soc.,* **77,** 437–471.

Karoly, D. J., 1990: The role of transient eddies in low-frequency zonal variations in the Southern Hemisphere circulation. *Tellus,* **42A,** 41–50.

Kidson, J. W., 1988: Indices of the Southern Hemisphere zonal wind. *J. Climate,* **1,** 183–194.

Kodera, K., M. Chiba, K. Yamazaki, and K. Shibata, 1991: A possible influence of the polar night stratospheric jet on the subtropical tropospheric jet. *J. Meteor. Soc. Japan,* **69,** 715–721.

Lau, N.-C., and M. J. Nath, 1990: A general circulation model study of the atmospheric response to extratropical SST anomalies observed in 1950–79. *J. Climate,* **3,** 965–989.

Limpasuvan, V., and D. L. Hartmann, 1999: Eddies and the annular modes of climate variability. *Geophys. Res. Lett.,* **26,** 3133–3136.

Nigam, S., 1990: On the structure of variability of the observed tropospheric and stratospheric zonal-mean wind. *J. Atmos. Sci.,* **47,** 1799–1813.

——, and R. S. Lindzen, 1989: The sensitivity of stationary waves to variations in the basic state zonal flow. *J. Atmos. Sci.,* **46,** 1746–1768.

North, G. R., T. L. Bell, R. F. Cahalan, and F. J. Moeng, 1982: Sampling errors in the estimation of empirical orthogonal functions. *Mon. Wea. Rev.,* **110,** 699–706.

Robinson, W. A., 1991: The dynamics of the zonal index in a simple model of the atmosphere. *Tellus,* **43A,** 295–305.

Rodgers, J. C., 1984: Association between the North Atlantic oscillation and the Southern Oscillation in the Northern Hemisphere. *Mon. Wea. Rev.,* **112,** 1999–2015.

——, and H. van Loon, 1982: Spatial variability of sea level pressure and 500-mb height anomalies over the Southern Hemisphere. *Mon. Wea. Rev.,* **110,** 1375–1392.

Shiotani, M., 1990: Low-frequency variations of the zonal mean state of the Southern Hemisphere troposphere. *J. Meteor. Soc. Japan,* **68,** 461–470.

Thompson, D. W. J., and J. M. Wallace, 1998: The Arctic oscillation signature in the wintertime geopotential height and temperature fields. *Geophys. Res. Lett.,* **25,** 1297–1300.

——, and ——, 2000: Annual modes in the extratropical circulation. Part I: Month-to-month variability. *J. Climate,* **13,** 1000–1016.

——, ——, and G. Hegerl, 2000: Annual modes in the extratropical circulation. Part II: Trends. *J. Climate,* **13,** 1018–1036.

Ting, M., M. P. Hoerling, T. Xu, and A. Kumar, 1996: Northern Hemisphere teleconnection patterns during extreme phases of the zonal-mean circulation. *J. Climate,* **9,** 2614–2633.

Trenberth, K. E., 1984: Interannual variability of the Southern Hemisphere circulation: Representativeness of the year of the Global Weather Experiment. *Mon. Wea. Rev.,* **112,** 108–125.

Wallace, J. M., 2000: North Atlantic oscillation/annular mode: Two paradigms—one phenomenon. *Quart. J. Roy. Meteor. Soc.,* **126,** 791–805.

——, and H.-H. Hsu, 1985: Another look at the index cycle. *Tellus,* **37A,** 478–486.

Yoden, S., M. Shiotani, and I. Hirota, 1987: Multiple planetary flow regimes in the Southern Hemisphere. *J. Meteor. Soc. Japan,* **65,** 571–585.

Yu, J.-Y., and D. L. Hartmann, 1993: Zonal flow vacillation and eddy forcing in a simple GCM of the atmosphere. *J. Atmos. Sci.,* **50,** 3244–3259.